Selective Aggregation of Single-Walled Carbon Nanotubes Using the Large Optical Field Gradient of a Focused Laser Beam

Thomas Rodgers, Satoru Shoji,* Zouheir Sekkat,+ and Satoshi Kawata‡
Department of Applied Physics, Osaka University, Suita, Osaka, Japan
(Received 28 February 2008; published 18 September 2008)

We demonstrate the selective aggregation of single-walled carbon nanotubes by photon forces, using the large optical field gradient of a laser focused through a high numerical aperture objective lens. The nanotubes, dispersed in an aqueous solution with a surfactant, are detected via Raman scattering from the confocal volume of the optical trap. By using a visible-light laser for both trapping and detection, the dynamics of the radial breathing mode signal taken at short intervals shows an increase of a single breathing mode over time, indicating the increase in the density of only one species of tube in the focal volume. This result represents a significant step toward the development of techniques for the arbitrary manipulation and sorting of nanotubes by optical fields.

DOI: 10.1103/PhysRevLett.101.127402 PACS numbers: 78.67.Ch, 42.50.Wk, 78.30.Na

Single-walled carbon nanotubes (SWCNTs) are graphene sheets wrapped into tubes of various possible sizes and wrapping angles, which are classified by a ''chiral vector'' specifying their wrapping coordinates on the 2D hexagonal graphene lattice. SWCNTs show remarkable chirality dependant electronic, mechanical, and optical properties. Soon after their discovery in 1993 [1,2], it was shown that one-third of SWCNT chiralities are metallic, and the remaining two-thirds are semiconductors of varying band gaps [3–5]. This property has great potential for the design of new devices; however, a fundamental obstacle to many proposed applications of SWCNTs is that the production of SWCNTs can produce only random chiralities [6].

Sorting of SWCNTs has been shown to be possible by chemical methods on tubes dispersed in solution, with the preferential wrapping of some chiralities by DNA [7], the density differentiation by competing surfactants [8], and recently the wrapping of nanotubes with aromatic polymers [9] leading to great improvements in chirality purification. Manipulating tubes by electromagnetic fields has the potential for a more arbitrary selection of chiralities, due to the unique electronic band structure of each chirality, but this flexibility is currently at the expense of the precision of the aforementioned chemical techniques. Electrophoresis using ac electric fields has been shown to separate metallic from semiconducting tubes in solution, by exploiting the difference in the static polarizabilities of metallic and semiconducting species [10]. The manipulation of bundled nanotubes with laser tweezers has been demonstrated using standard microscopy techniques [11]. Optical forces have been observed on individual tubes fixed to a substrate, by electron microscopy and Raman scattering [12]. Well dispersed tubes in solution have been trapped and observed via fluorescence quenching and Raman scattering, where it was suggested that by using a near-infrared trapping laser it is possible to preferentially manipulate semiconducting tubes [13,14].

Here we report the first experimental evidence of a strong selectivity of optical trapping, giving preference to one species of SWCNT. We give an analysis of the dynamics of vibrational radial breathing modes as measured by Raman scattering from the optical trap volume. We use a confocal Raman laser trapping system, and a single laser line for trapping and Raman excitation. SWCNTs produced by the high pressure carbon-monoxide (HiPCO) method were well dispersed by ultrasonication in pure water and surfactant (Triton-X, Wako). HiPCO produced nanotubes were chosen as they contain a wide range of chiralities [6]. Bundled nanotubes were subsequently removed by centrifugation.

Figure 1 shows an outline of the experimental setup. We implemented our optical tweezer system using the 633 nm line of a helium neon (He:Ne) laser. The laser is expanded to fill the back aperture of a 1.35 NA (numerical aperture) (oil immersion) objective, which is used to obtain the large

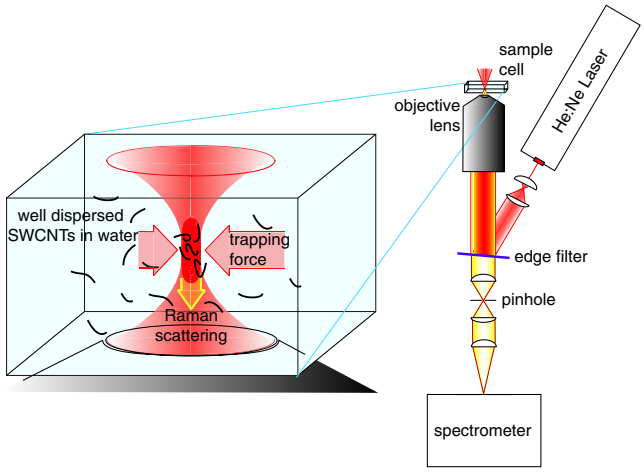

FIG. 1 (color online). The experimental setup for Raman trapping experiments. A He:Ne laser (633 nm) was used for both laser trapping and Raman excitation.

field gradient required for optical trapping. Laser power measured at the back aperture in this experiment was 8 mW. The laser was focused 10 μm deep into a 2 mm thick sample cell. A long wave pass edge filter (Semrock, RazorEdge) blocks the Raleigh scattered light while transmitting Stokes Raman scattered light to the detector. A confocal pinhole is used in the detection path to ensure that the Raman signal obtained comes only from the focal volume of the optical trap. The aggregation of SWCNTs in the optical trap was monitored by observing the strength of the Raman scattering from this volume. Measurements were recorded on a Spectra Pro 300i spectrometer (Acton Research) imaged with a liquid nitrogen-cooled charge-coupled device (CCD) array.

Combining Raman scattering with optical trapping offers vibrational information about a material in the optical trap. By using this method to monitor density dynamics of nanotubes in an optical trapping system we can gain detailed information about the relative populations of nanotubes inside the focal volume. Raman scattering is well known to be a highly resonant process for SWCNTs. In particular, the radial breathing modes (RBMs) allow us to estimate which chiralities of the tube are in the focal volume, by using an analysis from resonance Raman studies of SWCNTs [15,16]. Figure 2 shows a typical Raman spectrum of the RBMs in our sample (inset) and a calibration of the SWCNT concentration to Raman signal intensity. The main RBM peaks are marked with letters *A*, *B*, *C*, and *D*. Calibration of the Raman scattering intensity to the sample concentration was performed by diluting SWCNT solution with surfactant solution, and monitoring the amplitudes of these four main RBM peaks. This calibration was performed without confocality and with low NA optics to avoid trapping, and shows a linear relationship between the Raman signal intensity and the concentration of carbon nanotubes in the focal volume. Raman spectra were measured with 1 s CCD exposure time at intervals of 2 s, allowing full spectra to be recorded at each time step. Figure 3 shows the dynamics of RBM Raman scattering from SWCNT solution in our optical trap over a period of 10 min. The four main peaks are marked with *A*, *B*, *C*, and *D* as in Fig. 2. Peak *A* clearly shows more fluctuation than the other peaks *B*, *C*, or *D*, which remain relatively stable. This independent behavior of RBMs is evidence that the flux of nanotubes through the focal volume varies between species, implying that the larger SWCNTs (corresponding to lower frequency RBMs) experience a different force than the smaller tubes. The inset of Fig. 3 shows the peak amplitude of each of these RBM peaks plotted against time. There is a steady and marked increase in the amplitude of peak *A*, in clear contrast to the neighboring modes. This indicates aggregation of SWCNTs in the optical trap, where tubes of only one RBM are seen to be affected by the optical gradient force. Chiralities corresponding to these RBM peaks were assigned according to the Kataura plot method, using resonance Raman measurements of a similar sample [15,16]. By this method we estimate that the active peak may contain up to 4 nanotube chiralities, corresponding to the [11 8], [12 6], [13 4], and [14 2] chiral vectors, which are all metallic type SWCNTs, each of slightly different shift frequency ω_{RBM}. This active peak is seen, however, to be stable in frequency, around 196 cm^{-1}, suggesting that one metallic chirality is preferred in trapping. The inactive peaks correspond to semiconducting chiral vectors [10 3], [7 6], and [7 5]. A smaller

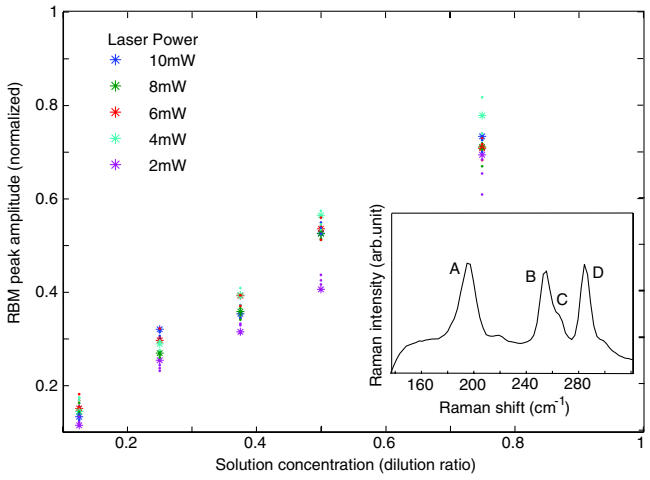

FIG. 2 (color online). Calibration of the Raman scattering intensity for radial breathing modes (RBMs) of metallic (asterisks) and semiconducting (dots) tubes, using various concentrations of SWCNT solution. Intensities are normalized to the full concentration of SWCNT + surfactant solution after dispersion. Inset shows a typical radial breathing mode RBM signal, with RBMs identified at 196 cm^{-1} (*A*), 255 cm^{-1} (*B*), 260 cm^{-1} (*C*), and 285 cm^{-1} (*D*).

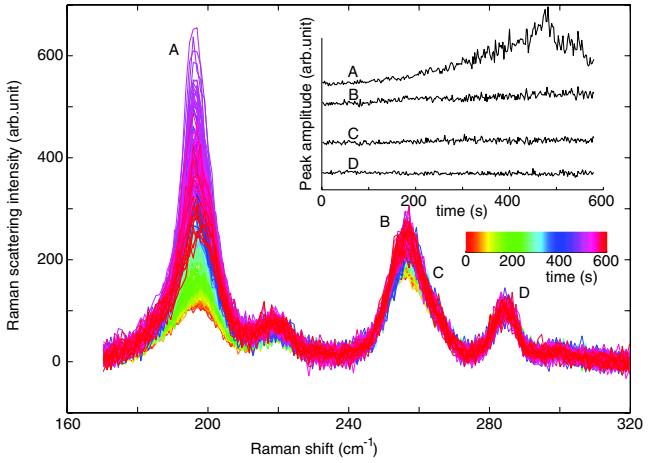

FIG. 3 (color online). The radial breathing mode dynamics of SWCNTs dispersed in solution, as measured by Raman scattering. This ensemble of 300 spectra was taken at intervals of 2 s, over a period of 10 min. Inset shows the dynamics over time of the signal intensities of the four peaks *A*, *B*, *C*, and *D*.

peak at 219 cm^{-1} showed strong dependence on solution centrifugation time, and is identified as a vibrational mode from remnant bundled SWCNTs that were not removed during sample preparation [17]. A weak vibration at 300 cm^{-1} can be assigned to the RBM of the [8 3] nanotube [15], although the weakness of this signal does not allow us to resolve significant changes in density of these SWCNTs. An increase in the intensity of one RBM peak over time indicates an increase in density in the optical trap of one or a just small set of chiralities, despite no increase in the density of other SWCNTs. From our density calibrations shown in Fig. 2, this increase in Raman scattering signal represents a fivefold increase in the concentration of this species of tube in the optical trap. Studies performed by Tan and colleagues [13,14] showed an enhancement of semiconducting tubes by a near-infrared laser trap of 1064 nm wavelength, while probing with 785 nm for Raman scattering excitation. Moreover, the size of the preferentially trapped tubes in that report is smaller than other RBMs visible under 785 nm excitation, in contrast to our experiment where larger diameter, metallic tubes are shown to be trapped. In this, our experiment compliments the previous work by showing strong trapping enhancement of tubes different in both size and conductivity, and extends it by reporting the first experimental evidence of a wavelength dependant selectivity for laser trapping.

As all tube species in our experiment are subject to the same optical field gradient, this result highlights the difference in polarizabilities of different SWCNTs at this wavelength. In a focused beam 3D laser tweezer system, the optical gradient force required for trapping arises from dipole induction in the object by the electric field, and must compete with photon momentum transfer due to scattering and absorption, and also with Brownian motion to achieve a stable trapping potential [18]. For materials with positive polarizability, the gradient force acts in the direction of increasing field gradient, whereas photon momentum transfer acts in the direction of light propagation, and Brownian forces are nondirectional. The forces acting on a particle can be written

$$F(r) = \alpha \frac{n_m}{2c} \nabla E^2(r) + F_{\mathrm{PM}} + F_B, \qquad (1)$$

where α is the tensor of polarizability, n_m is the refractive index of the immersion medium, E is the electric field vector, and F_{PM} and F_B are the photon momentum and Brownian forces, respectively. Significantly, α, the tensor of polarizability, is a function of the excitation wavelength. To analyze the polarizabilities for the SWCNTs observed in this experiment, we performed qualitative analysis of the real and imaginary parts of the dielectric constant of the SWCNT we observed in our experiment. We assume that the imaginary part of the dielectric constant is in proportion to the joint density of states, which was calculated by a tight-binding model [4,5]. The real part of the dielectric constant is derived from the imaginary part according to the Kramers-Kronig relation. Figure 4 shows the real and imaginary parts of the dielectric constant calculated by this method, separating the seven chiralities seen in our experiment into semiconducting and metallic groups. A dotted line marks the 633 nm laser line that is used in our experiments. These refer only to the elements of the dielectric tensor along the tube axis, as the dielectric constant perpendicular to the tube axis is so small as to be negligible. The polarizability is a function of the real part of the dielectric constant, and so the peaks of that function can give us an insight into the enhancement of the trapping force on a given chirality for a given wavelength. In contrast, the imaginary part of the dielectric function is proportional to absorption, and so contributes only to antitrapping forces by heating and photon momentum. As a first approximation, we can estimate the relative trapability of the chiralities by comparing the relative intensities of the calculated dielectric function at the trapping wavelength, 633 nm. Among the semiconducting tubes, it is clear that the [10 3] and the [7 5] tubes have a low dipole polarizability, and the [7 6] tube lies on the edge of our calculated resonance. These semiconducting tubes all have large values for the imaginary part of the dielectric constant, corresponding to optical absorption. For the metallic nanotubes, [12 6] [13 4], and [14 2] all show higher dipole polarizability as well as lower absorption than their semiconducting counterparts. For more quantitative analysis of the resonance positions and their relative strengths at a given wavelength, excitonic and curvature effects can be

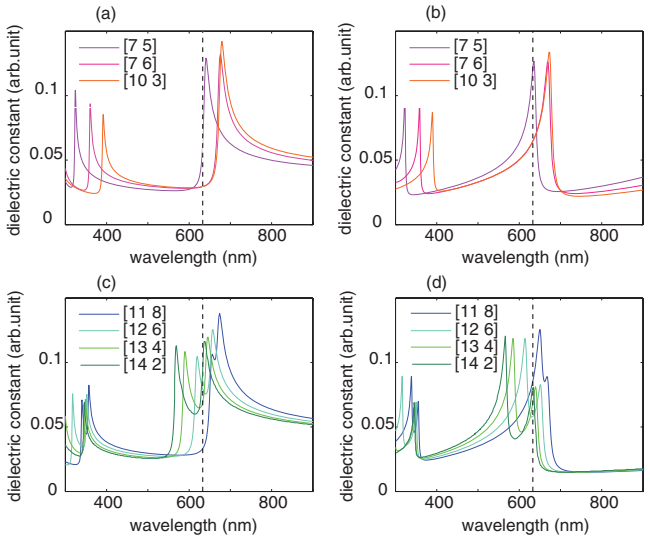

FIG. 4 (color online). Calculated dielectric function of the 6 chiralities of SWCNT that are observable in our experiment. The upper figures [(a) and (b)] show the real and imaginary parts of the dielectric function, respectively, for the semiconducting chiralities [7 5], [7 6], and [10 3]. Lower figures [(c) and (d)] show the real and imaginary parts of the dielectric function of the metallic species with chiral indices [14 2], [13 4], [12 6], and [11,8]. Guides for the eye show the 633 nm laser line.

considered in the initial band-structure calculations [16]. It should be noted that our detection method, Raman scattering, is also a resonant process, and for a given laser line only a small selection of SWCNT RBM signals are observable even from a sample containing a very wide range of chiral species. Indeed, the selectivity of Raman resonance is due to the characteristic optical transitions of each SWCNT chirality, and it is this property that allows us to assign chiral species from RBM frequency and excitation energy. Our experimental result shows a number of RBMs, so there may be a misconception that all tubes under resonant Raman scattering should experience enhancement of the optical gradient force. However, the resonance linewidth for Raman scattering, as a superposition of incoming and outgoing resonances, is broad compared to the requirement of high polarizability and low absorption needed for laser trapping to overcome Brownian motion [19]. Measurements of polarizability via the Raleigh scattering spectra of SWCNTs [20] show good agreement to the line profile of our calculated dielectric function, characterized by sharp, well-defined and nonsymmetric peaks. This difference between the broad resonance profile for Raman scattering and the narrower resonance profiles for trapping enhancement allows us to observe trapping enhancement for one species of tube in a sample for which many species show resonant Raman scattering. Our study has demonstrated that the selective aggregation of tubes in an optical trap is a strong indication that the trapping forces on different species of tubes are highly wavelength dependent. This wavelength dependence can be exploited for selectively enhancing the trapping force on individual species of nanotube, for the separation and sorting of SWCNTs. There is great potential for nanotube processing, and it is expected that by changing the wavelength of the trapping laser, different chiralities of nanotube will be subject to enhancement of the optical trapping force.

The authors thank Remo Proietti Zaccaria, Takaaki Yano, and Sana Nakanishi for helpful discussions. This research was supported by CREST, Japan Science and Technology Corporation (JST), and by the Grant-in-Aid for Young Scientists, The Ministry of Education, Culture, Sports, Science and Technology, Japan.

*shoji@ap.eng.osaka-u.ac.jp

[+]Permanent address: The Institute of Nanomaterials and Nanotechnology (INANOTECH), Rabat, Morocco; and Hassan II Academy of Science and Technology, Rabat, Morocco.

[‡]Permanent address: Department of Applied Physics, Osaka University, Suita, Osaka, Japan; and Nanophotonics Laboratory, RIKEN, Wako, Saitama, Japan.

[1] S. Iijima and T. Ichihashi, Nature (London) **363**, 603 (1993).
[2] D. S. Bethune *et al.*, Nature (London) **363**, 605 (1993).
[3] N. Hamada *et al.*, Phys. Rev. Lett. **68**, 1579 (1992).
[4] R. Saito *et al.*, Appl. Phys. Lett. **60**, 2204 (1992).
[5] T. Ando, J. Phys. Soc. Jpn. **74**, 777 (2005).
[6] P. Nikolaev *et al.*, Chem. Phys. Lett. **313**, 91 (1999).
[7] M. Zheng *et al.*, Science **302**, 1545 (2003).
[8] M. S. Arnold *et al.*, Nature Nanotech. **1**, 60 (2006).
[9] A. Nish *et al.*, Nature Nanotech. **2**, 640 (2007).
[10] R. Krupke *et al.*, Science **301**, 344 (2003).
[11] J. Plewa *et al.*, Opt. Express **12**, 1978 (2004).
[12] K. Kaminska *et al.*, Phys. Rev. B **73**, 235410 (2006).
[13] S. Tan *et al.*, Nano Lett. **4**, 1415 (2004).
[14] S. Tan *et al.*, Proc. SPIE Int. Soc. Opt. Eng. **5593**, 73 (2004).
[15] J. Maultzsch *et al.*, Phys. Rev. B **72**, 205438 (2005).
[16] A. Jorio *et al.*, Phys. Rev. B **72**, 075207 (2005).
[17] H. Kataura *et al.*, in *Proceedings of the XIV International Winterschool/Euroconference, Kirchberg, Tirol, Austria, 2000*, AIP Conf. Proc. No. 544 (AIP, New York, 2000), pp. 262–265.
[18] A. Rohrbach and E. Stelzer, J. Opt. Soc. Am. A **18**, 839 (2001).
[19] T. J. Davis, Opt. Express **15**, 2702 (2007).
[20] M. Sfeir *et al.*, Science **306**, 1540 (2004).